2.2 Deformable Mirrors

Kyle Van Gorkom

1. Introduction

MagAO-X employs two deformable mirrors (DMs) for common-path wavefront control in a woofer-tweeter scheme and a third downstream of the AO loop dedicated to non-common-path correction (NCPC). The system woofer, a high-stroke 11x11 97-actuator deformable mirror from ALPAO, will provide low-order wavefront correction while the tweeter, a 50x50 2040-actuator DM from BMC provides the high-order wavefront correction. A pyramid wavefront sensor (PyWFS) operating at 3.63 kHz will drive these DMs. The NCPC DM is a second ALPAO DM97 that will perform the NCP correction in concert with low-order and focal-plane wavefront-sensing in the science path. All three DMs were characterized, calibrated, and flattened in front of a Zygo Verifire interferometer prior to integration into the MagAO-X instrument. In Sec. 2, we describe the safety procedures to be followed when handling the DMs. In Sec. 3, we lay out the cabling procedure to be followed at LCO and an algorithm for validation of actuator functionality after cabling. In Sec. 4, the results of DM characterization and their comparison to design specifications are presented. Finally, in Sec. 5, we describe a procedure for minimizing static instrument aberrations and estimate the current instrument Strehl.

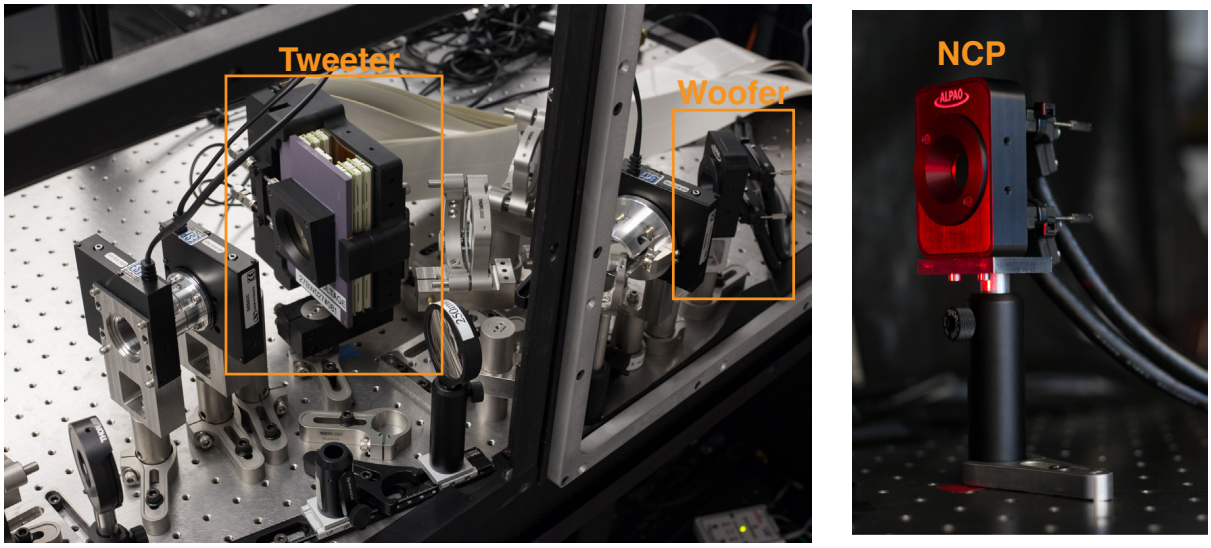

Fig. 1.—: Left: The tweeter and woofer integrated in MagAO-X. Right: The NCPC DM prior to integration.

2. DM Operations & Safety

MEMS DMs are subject to two common failure modes: oxidation through humidity damage and "snap-down" of actuators from voltage events which exceed some threshold.

To mitigate humidity damage, we will drive the 2K DM only when relative humidity is under 15%. To achieve this, we have built a dry air system that maintains low-humidity and partial vacuum within the DM chamber. The system reports the humidity reading to the user and produces a warning when the relative humidity exceeds the operating threshold and an automatic shutdown above the safety threshold. In the event of a glitch in the dry air system, the DM chamber can be kept in safe operating conditions with a N2 bottle and a humidity sensor on the chamber exhaust.

Snap-down has two main causes: an off-limits voltage sent to the DM by the drive electronics or an electro-static discharge (ESD) event. BMC has reported 210 V as the maximum safe command to be sent to the 2K DM. This limit is enforced at multiple levels: the MagAO-X software clips commands to 210 V, the BMC software also limits commands to safe limits, and the drive electronics has a built-in hardware limit. ESD events can be prevented by safe handling procedures. All operators will wear ESD wrist straps and grounding heel straps whenever handling the 2K DM, its cables, or the drive electronics. The wrist straps will be hooked to an ESD monitor which gives an audible and visual alarm when an operator becomes ungrounded. The ESD monitor can be additionally hooked to the table or a grounding mat for additional safety. The MagAO-X table and the electronics rack will each be separately grounded. To prevent any build-up of electric potential between the electronics rack and the instrument, a grounding wire will be run between the two.

The ALPAO DMs have no reported humidity thresholds for safe operation and are much less sensitive to ESD events. Nevertheless, to prevent any potential damage, wrist straps will be worn while handling the ALPAO DMs. Commands are clipped to operating limits in the same way as for the BMC DM. Additionally, powering off a DM while voltage or current is applied to the DM has been reported as a cause of damage. To prevent this, the MagAO-X software will not send a command to power off a DM unless it has been sent a "zero" command and the connection has been released. UPS battery backups will allow for safe shutdown of DMs in the event of a power outage.

3. DM Cabling Procedures

The cables between the DM driver electronics and the mirrors were designed as a two-step system, allowing the cables to be disconnected for shipment at the feed-through port on the MagAO-X bench rather than in the electronics rack or at the DMs on the instrument table. After the instrument is moved onto the Nasmyth platform, all the cables between the DM drivers in the electronics rack and the cable pass-through on the instrument table will need to be reconnected. After making the connections, a simple python script will enable rapid validation of actuator functionality. All DM safety procedures described

in Sec. 2 will be followed during the cabling process. The required equipment, cabling procedure, and functional validation are described in Sec. 3.1-3.3.

3.1. Required Equipment

The following items will be brought to LCO for use in cabling and handling the DMs after unpacking the instrument:

- ESD wrist straps
- ESD heel grounding straps
- ESD monitor
- Latex gloves
- Acetone
- Isopropyl alcohol (IPA)
- Air duster
- Tex wipes
- Wiha chip lifter
- Mini pocket pry bar
- Flathead screwdriver
- Spare 2K Samtec connectors
- Spare 2K interconnect board
- Spare 2K cables

3.2. Cabling Steps

On the two ALPAO DMs, the connection at the feed-through is a standard SCSI, so cabling the ALPAOs at LCO will be straight-forward. On the BMC 2K, this connection is a set of 4 total Samtec connectors on 2 interconnect boards. The procedure for recabling the 2K is described on the following pages (BMC Hardware Assembly Procedure Document 2018).

Although not expected, in case the connections at the driver or DM housing must be remade at LCO, the BMC manual describing these procedures will be available both in printed and PDF formats.

2. Interconnect Board Samtec Connection Procedure

2.1 Interconnect Board Samtec Connector Preparation and Installation

2.1.1 Loosen and take off the 4 thumb screws on the cover plate for the Samtec connector. See Figures 2 and 3. If there is more than one Samtec connection, start by attaching the connection farthest from the yellow plate. Remove the cover plate and set it aside.

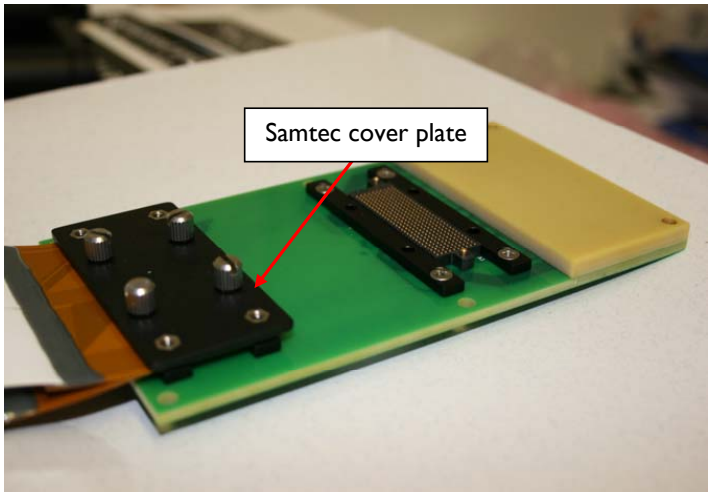

Figure 2. Interconnect board on grounded table.

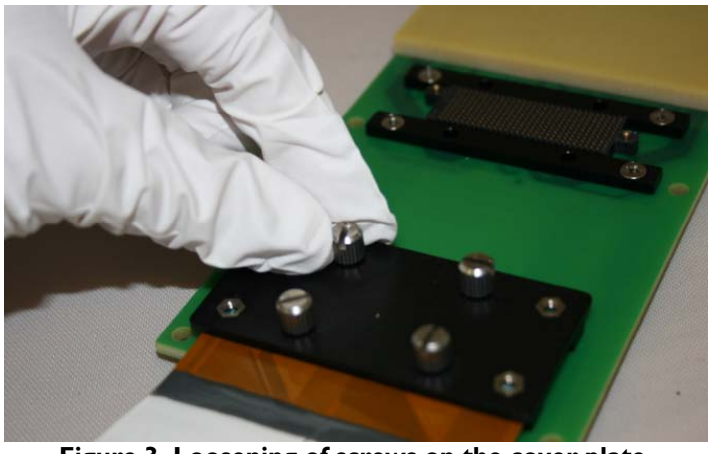

Figure 3. Loosening of screws on the cover plate.

2.1.2 Once the cover plate is removed, a gold connection plate is revealed, as shown in Figure 4. Remove the Samtec connector. The Samtec connector on the interconnect board can be seen in Figure 8.

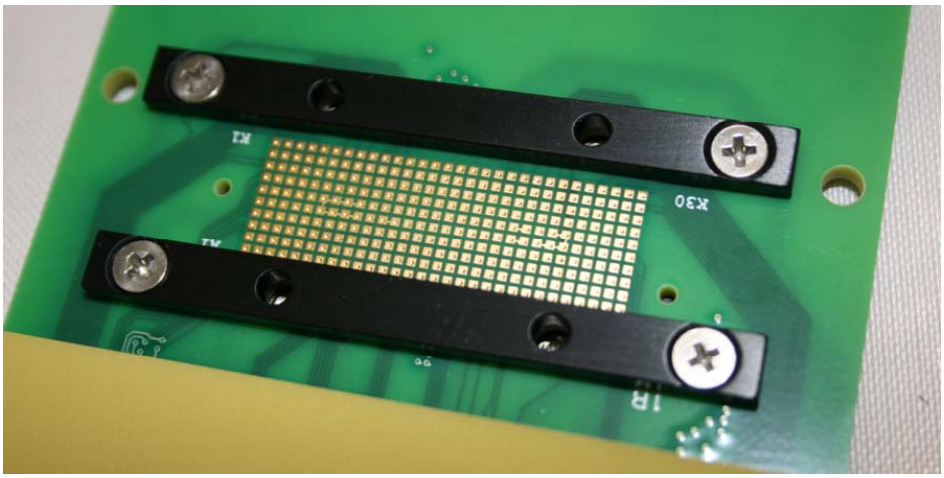

Figure 4. Gold connection plate.

2.1.3 Using a Tex wipe, gently wipe the connector first with Acetone and then with IPA. Only wipe in ONE direction. See Figure 5.

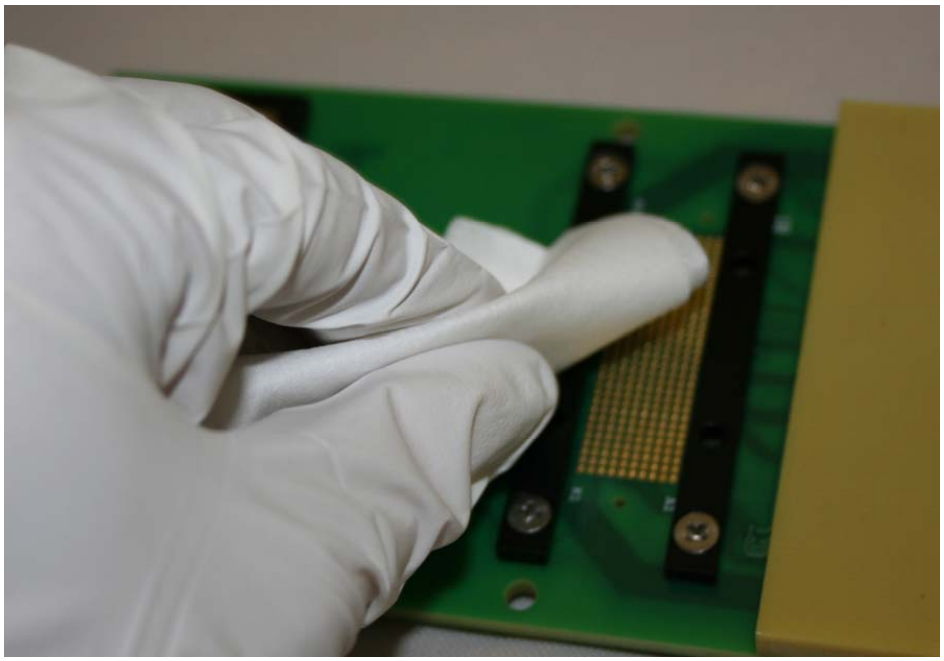

Figure 5. Wiping the Samtec connector with Tex wipe.

2.1.4 Repeat step 2.1.3 for the gold-covered side of the Samtec end of the cable, as shown in Figure 6, to be connected to the Samtec connector.

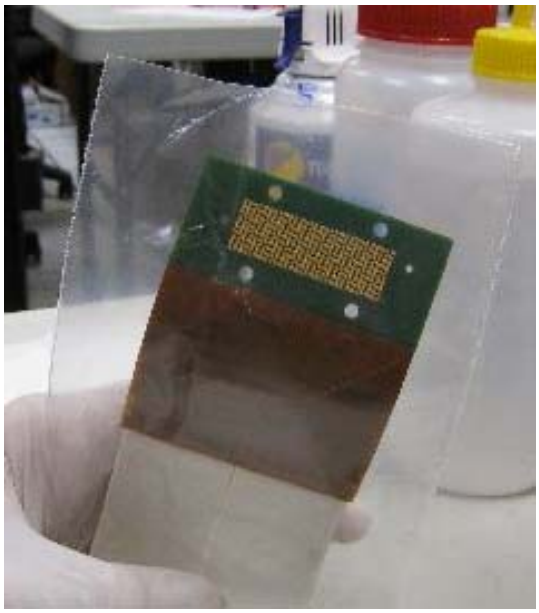

Figure 6. Gold-covered side of the Samtec end of the cable.

2.1.5 Use the air duster to blow-dry both gold-covered connections: on the Samtec connector and on the gold-covered part of the end of the cable. See Figure 7.

Figure 7. Blow dry both gold-covered connections with an air duster.

2.1.6 Place Samtec connector onto the interconnect board. There is only one orientation that will fit, with the alignment pins of the Samtec connector inserted to the alignment holes on the interconnect board. See Figures 8 and 9.

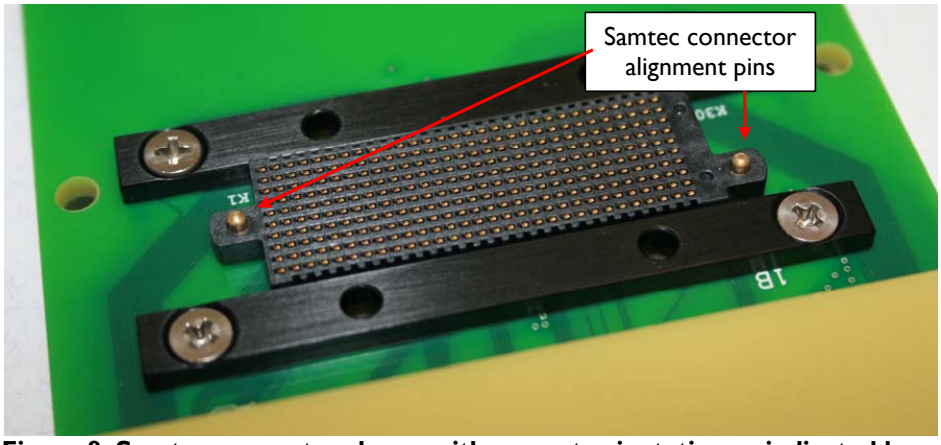

Figure 8. Samtec connector shown with correct orientation as indicated by alignment pins.

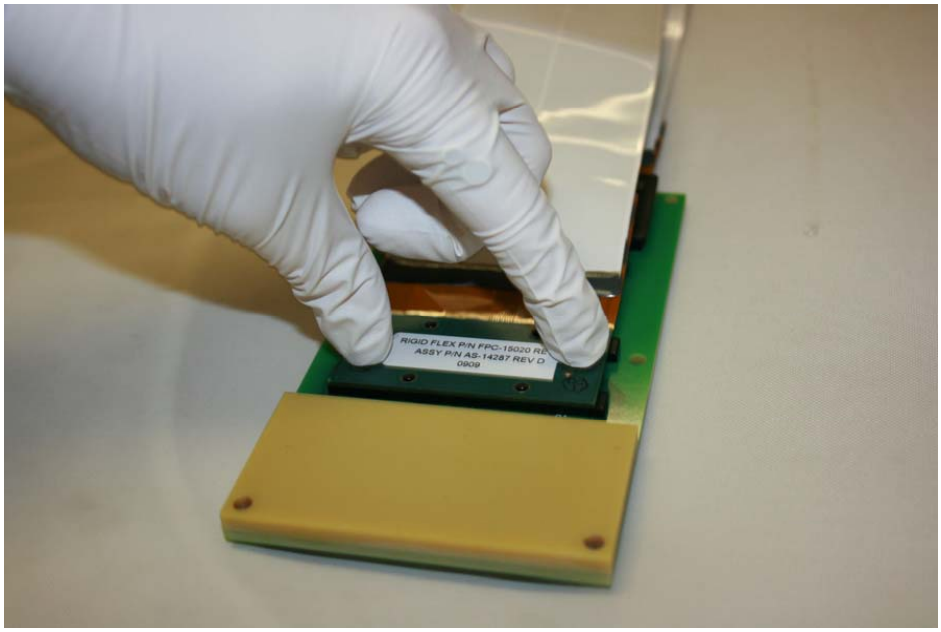

Figure 9. Place cable connector on top of Samtec connector.

2.1.7 Place the cover plate over the connection and tighten screws in X-pattern, starting with the top right (1) following in numerical order (2-4). See Figure 10.

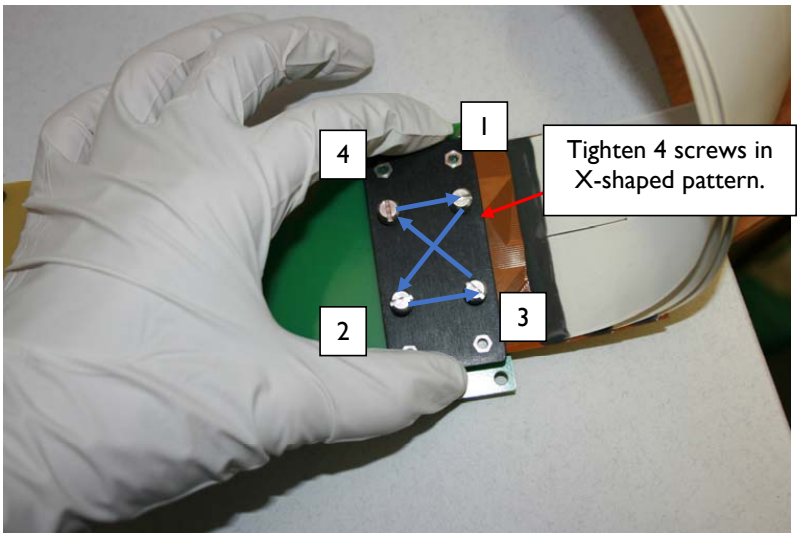

Figure 10. Tighten the cover plate over the connection in an X-pattern.

2.1.8 Repeat Procedure 2.1 for any subsequent Samtec connections on the interconnect board until complete. Please also allow smooth flow of the Kilo cables as the Samtec connectors are being installed.

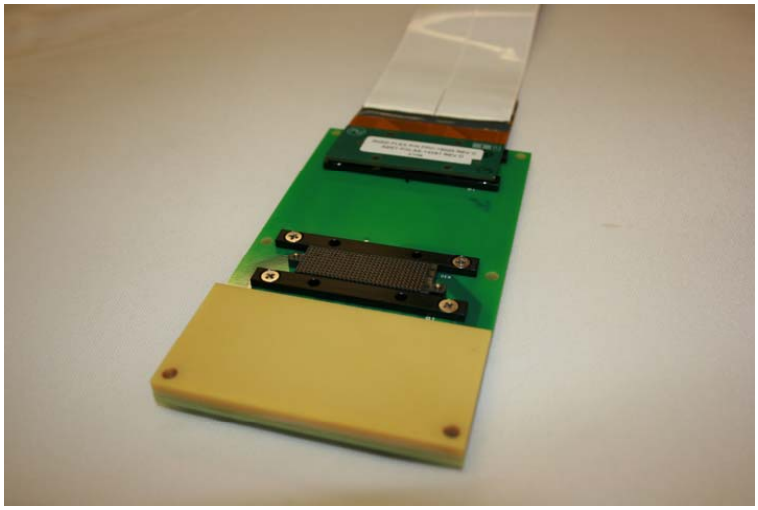

Figure 11. Completed installation of one Samtec connector to interconnect board.

3.3. Validation of actuator functionality

Any time the DMs are recabled, there is a risk that the connections were not made properly, resulting in nonresponsive, coupled, or otherwise anomalous actuator behavior. To assess actuator functionality, we have developed the following procedure:

1. Using the `cacao` software, build a Hadamard interaction matrix for each DM with an internal source
2. Read the `zrespM` FITS output into a python script `validate_actuators` and compute the RMS response for each acutator
3. Display the actuator response for each DM

An example output is shown in Fig. 2. Non-responsive actuators show up in deep blue, while strongly responsive actuators show up in yellow. This figure serves as the baseline nominal behavior for the 2K. The known coupled actuators show up in yellow, while actuators in the vicinity of the bump show a limited response. The pupil shape and low-order variations across the DM are a result of the illumination on the DM. Any localized changes from this image indicate a change in actuator functionality. An Excel spreadsheet provided by BMC will let us map the actuator to the corresponding cable, enabling us to quickly isolate any troublesome connections.

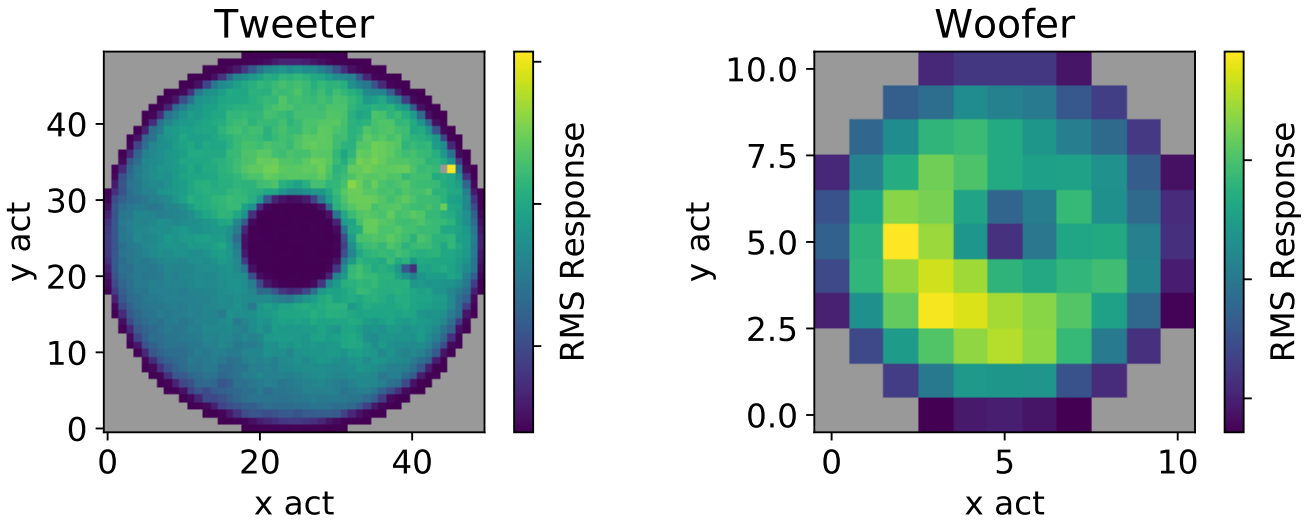

Fig. 2.—: Metric to validate actuator functionality after cabling at LCO. Coupled actuators show up as bright features while non- and less-responsive actuators show up as dark features.

4. DM Characterization

The characterization testbed employed a Zygo Verifire, a Fizeau-type interferometer, to make DM surface measurements. To reduce static aberrations, the collimated reference and test wavefronts were created with a 4 inch, $\lambda/50$ (PV) Dynaflect transmission flat. The Verifire natively supports up to 6x zoom, but some characterization activities required additional resolution to resolve the fringes created by high-stroke commands. To increase the resolution, we placed a two-lens beam reducer in the collimated beam between the interferometer and DM, which created an additional 6x - 20x improvement in resolution.

To expedite the measurement process, we wrote a Python library that automates the interferometer measurements and DM commands and synchronizes the process across multiple servers via a shared network drive. Zygo provides a Python API for measurement acquisition, basic post-processing, and writing to disk. Each DM has a custom API, which we interfaced with the Compute and Control for Adaptive Optics (CACAO) package for low-latency DM control. For any desired characterization procedure, the code accepts a list of DM command inputs and iterates over the list in a command-measure loop. The code is available on github at https://github.com/magao-x/zygo-automation. A schematic of the testbed is shown in Fig. 3.

To form the testbed interaction matrix, measurements of positive and negative influence functions (IFs) were made. For the 2K, grids of IFs were poked simultaneously to accelerate the measurement process. Multiple measurements were averaged and the static surface of the DM was removed to reduce noise. The interaction matrix was inverted, and DM flats were created in closed loop with the Zygo.

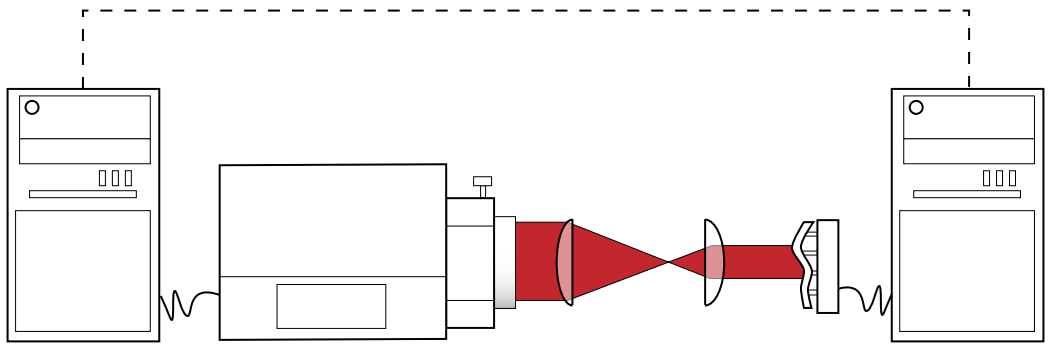

Fig. 3.—: All three DMs were characterized with a Zygo Verifire interferometer. A beam expander between the Zygo and DM provided additional resolution when necessary. Measurements and commands were synced between the Zygo PC and DM control computer via a shared network drive.

4.1. Tweeter Characterization

The system tweeter is a 2040-actuator 3.5 μm stroke MEMS DM from Boston Micromachines Corp. The actuator grid is on a 400 μm pitch inscribed in a 19.6 mm diameter aperture. The reflective membrane has a gold coating, and the device is environmentally sealed behind an AR-coated window with a 6° wedge. The maximum safe voltage is capped at 210 V. This is a 100% yield (no stuck or nonresponsive actuators) device with a few notable flaws: 2 actuators are coupled (they both respond to a voltage applied to either one), and a bump on the surface grows with voltage bias up to a maximum peak of 0.86 μm and a width of 1.4 mm. These features are shown in Fig. 5.

The closed-loop flat defined in front of the Zygo is shown in Fig. 6. Over the active aperture of the DM, the surface has 12.6 nm RMS, or 8.1 nm RMS with the bump masked. Over the coronagraphic pupil, the RMS reduces to 6.9 nm or 0.5 nm RMS within the control band of the DM. All figures are given in surface error rather than wavefront.

The choice of 2K operating bias has significant implications for the available stroke and chance of saturation during AO operations. We examine 3 stroke metrics in order to evaluate 2K performance and adopt an operational bias. The first, single-actuator stroke, describes the full range of surface deflection from a bias position when a single actuator is released (0 V) and then subsequently railed (210 V). The deflection in the two directions is highly asymmetric for most bias positions (and entirely one-sided at 0 and 210 V); since motion in both directions is operationally important, we capture the effective dynamic range of the surface deflection by taking the stroke s to be twice the smaller of the two deflections:

$$s = 2 \times \min(|s_{\text{railed}}|,\ |s_{\text{released}}|) \tag{1}$$

Flat Surface Error (nm RMS)

	Designed		As-Built	
	Max Spec.	Typical Spec.	Actual (Clear Aperture)	Actual (Coronagraph)
Tweeter	20	13	**8.2***	**6.9**
Woofer	7	4	**2.6**	**2.1**
NCP	7	4	**5.1**	**2.2**

Fig. 4.—: Comparison of budgeted to as-built DM surface quality. In all cases, the as-built DMs exceed design specifications.

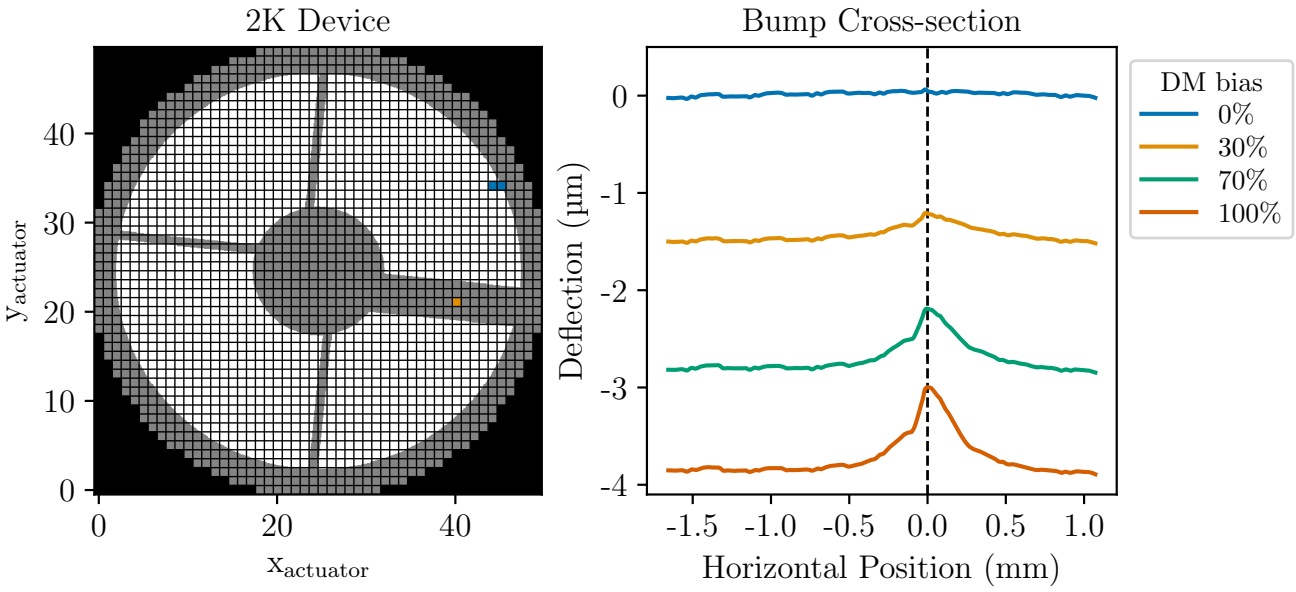

Fig. 5.—: Left: Map of the 2K actuator grid with overlaid coronagraphic pupil. The two coupled actuators are indicated in blue. The orange actuator is nearest the bump. Right: The behavior of the bump as the DM surface is pistoned.

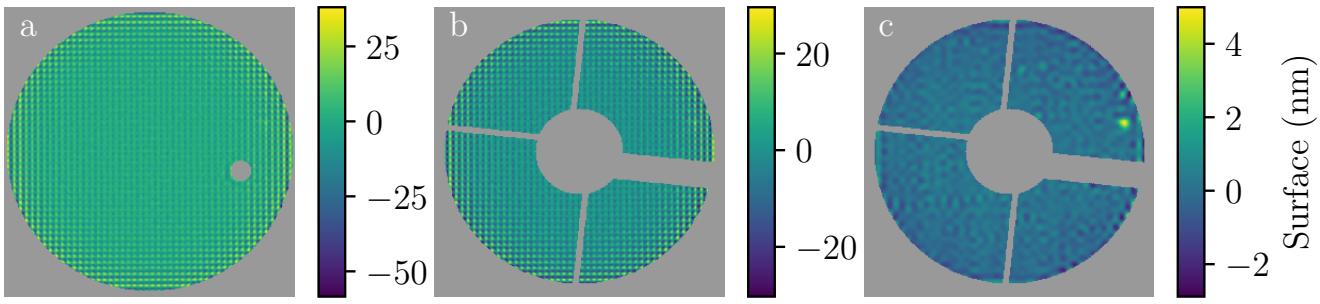

Fig. 6.—: Tweeter Flats. (a) The best flat achieved 12.6 nm RMS over the full DM aperture and 8.1 nm RMS after masking the bump. (b) In the vAPP pupil, the flat is 6.9 nm RMS. (c) The in-band flat in the vAPP pupil is reduced to ~ 0.5 nm RMS.

Inter-actuator stroke measures the surface peak-to-valley (PV) of two neighboring actuators when one is railed and the other released, and global stroke captures the range of surface deflection when all actuators are released and railed together, with the same symmetry constraint applied to both metrics. We measured these stroke metrics in detail for 10 actuators distributed across the DM surface and found similar behaviors for all. The median of each of these curves is plotted in Fig. 7. Global stroke peaks at $\sim$ 40% bias at $\sim$ 4μm, while single- and inter-actuator stroke peak at $\sim$ 70% bias at 1.2 and 1.0 μm, respectively. Inter-actuator stroke places an upper limit on the amplitude of the highest spatial frequencies that can be corrected with the tweeter and drives the choice of operational bias to 70%.

The unpowered device has low-order sag as a result of fabrication processes. When the DM is commanded to a flat at 70% bias, a range of voltages from 60 to 80% is required to drive out the sag. As a result, a large fraction of the actuators are at a non-optimal bias for single- and inter-actuator stroke. If, however, the $\sim$ 100nm of static tweeter sag is offloaded to the woofer and only high-order static errors are corrected on the 2K, the range of voltages in the flat bias can be narrowed about the optimal point, driving single- and inter-actuator stroke up across the full DM. In this scenario, $>$ 99% of the actuators exceed the 0.85μm design specification for inter-actuator stroke. See Fig. 8.

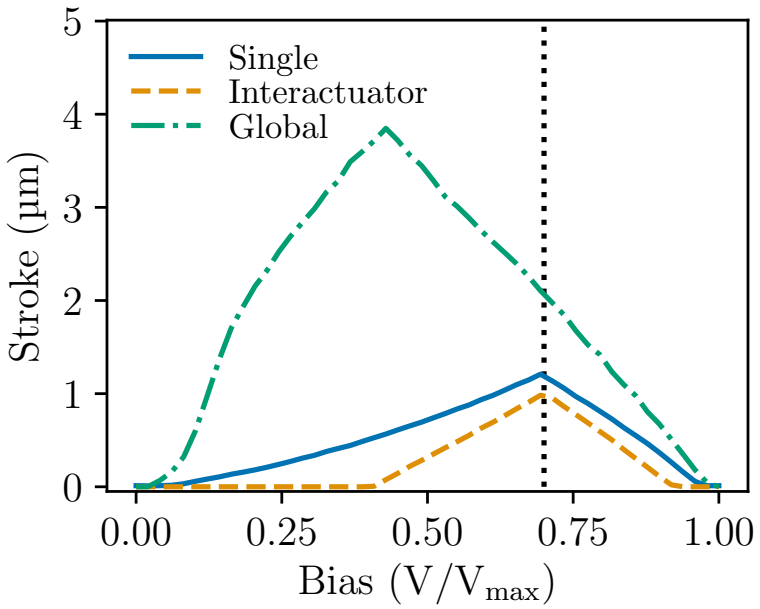

Fig. 7.—: Stroke on the tweeter DM as a function of voltage bias. Inter-actuator stroke peaks at 70% bias with a value of 1 μm. Values are reported in surface.

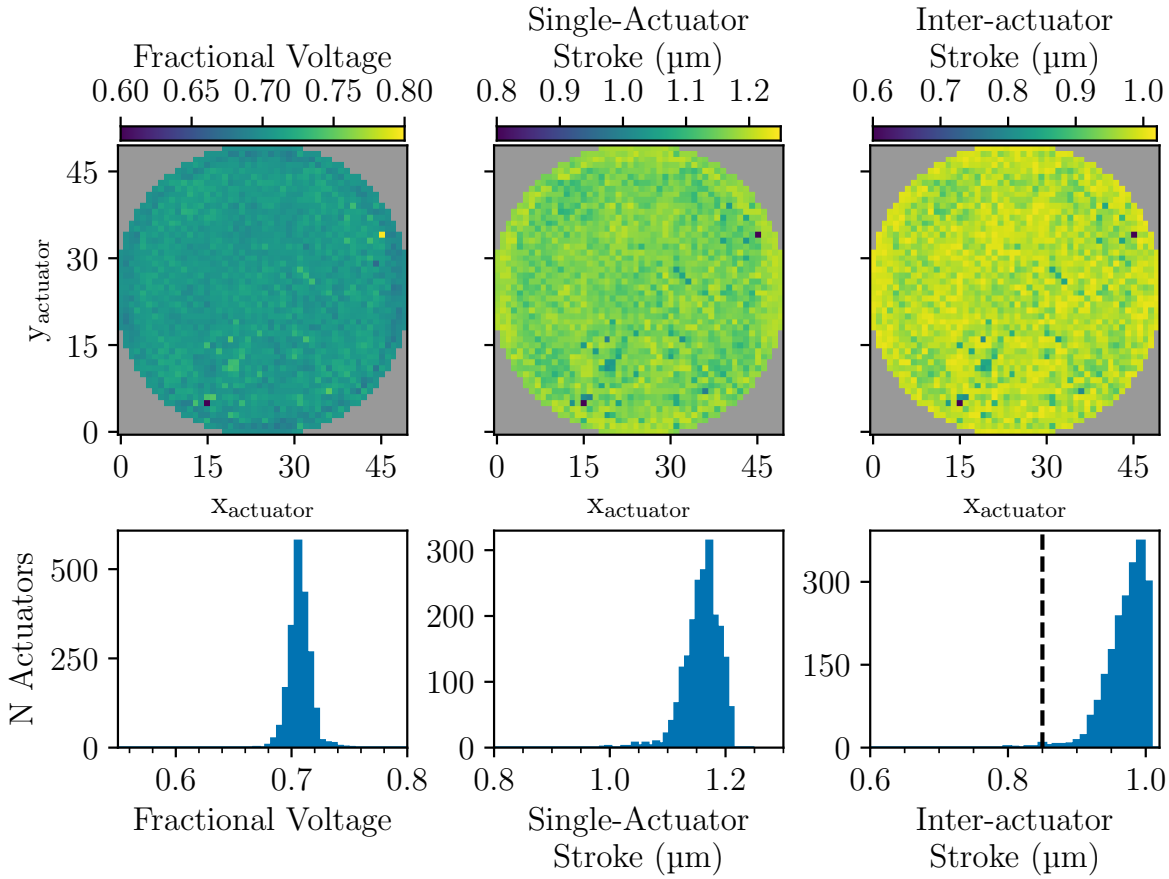

Fig. 8.—: Voltage and stroke maps for the "relaxed" 2K flat. 100nm RMS of low-order surface (mostly defocus and astigmatism) is offloaded to the woofer. $> 99\%$ of actuators exceed 0.85 μm of inter-actuator stroke.

4.2. ALPAO Characterization

The woofer and NCPC DMs are two ALPAO DM97 devices, each with 97 actuators arranged in an 11x11 grid. The DMs are compact voice coil continuous facesheet deformable mirrors with a 13.5 mm aperture and actuators on a 1.5 mm pitch.

These are high-stroke devices, capable of $\sim 12-15\mu$m surface P-V of tip/tilt and $\geq 10\mu$m surface P-V of low-order Zernike modes (see Fig. 9). The woofer has 2.24 μm inter-actuator stroke (in surface) while the NCPC has 1.52 μm. Both devices can be run at > 2 kHz.

The ALPAO flats are of very high quality. Over the full DM aperture, the woofer achieves of flat of 2.6 nm RMS, while the NCPC DM achieves a slightly higher error of 4.9 nm RMS. Over the vAPP pupil projected onto the DM surfaces, these flats reduce to $\sim$ 2nm RMS. Within the control radius of the

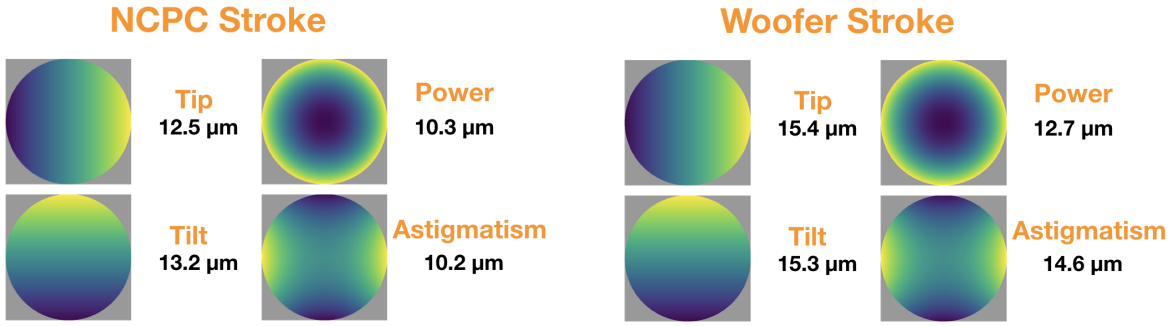

Fig. 9.—: Low-order stroke limits for the NCPC and woofer DMs, given in PV of surface (ALPAO test reports).

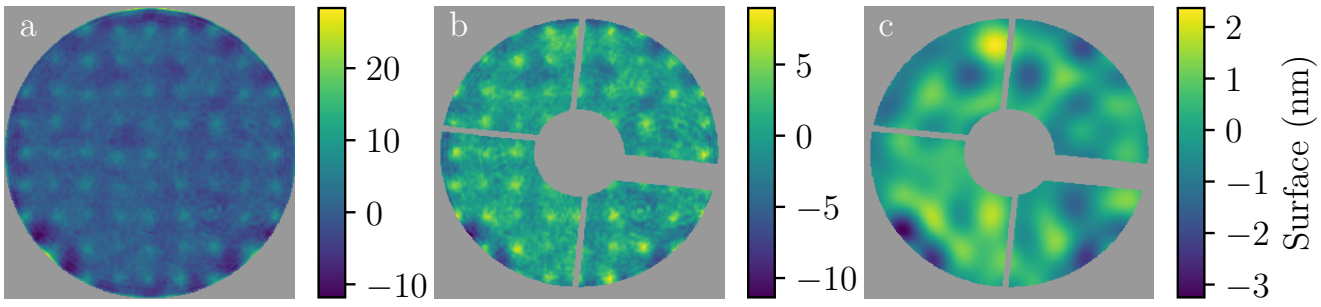

Fig. 10.—: Closed-loop flat on the woofer over (a) the full surface, (b) the vAPP pupil projected onto the DM, and (c) the vAPP pupil within the DM control radius. The flat has an RMS of 2.6 nm over the full surface, 2.1 nm over the vAPP pupil, and 0.7 nm RMS in-band.

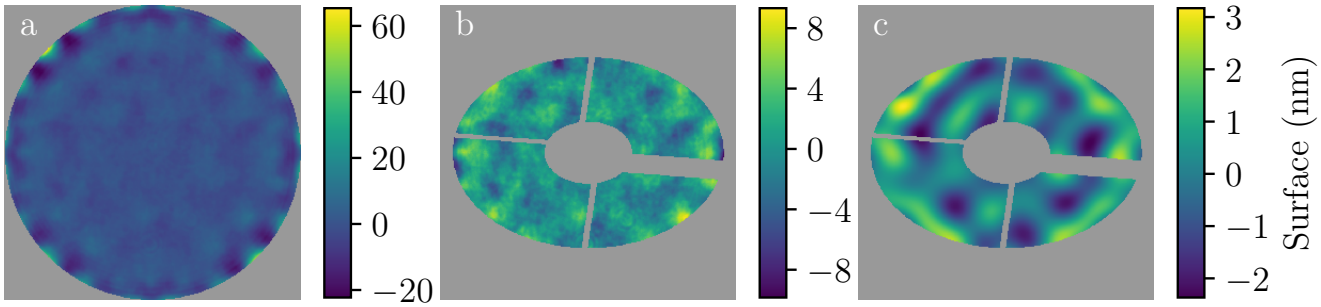

Fig. 11.—: Closed-loop flat on the NCP DM over (a) the full surface, (b) the vAPP pupil projected onto the DM,and (c) the vAPP pupil within the DM control radius. The flat has an RMS of 4.9 nm over the full surface, 2.2 nm over the vAPP pupil, and 0.8 nm RMS in-band.

ALPAO DMs, the flat error is 0.7 and 0.8 nm RMS for the woofer and NCPC, respectively. See Fig. 10 and 11.

The surface shape of ALPAO DMs have been noted to retain a trace of previous shapes on the DM for minutes to hours afterwards, an effect known as creep (Bitenc 2010 and 2017). ALPAO attributes this behavior to the polymer material used on the underlying actuator plate. Bitenc et al. developed a software compensation for creep that takes into account the history of commands placed on the DM and applies a time-dependent correction factor. Bitenc (2017) also identified an independent source of surface error, credited to the heating of the electrical elements that drive the DM.

In closed loop, creep is corrected as it arises, so we do not anticipate the need for a compensation scheme on the system woofer or the NCP DM in most observing modes. In some modes, however, we may want to maintain the NCP DM in a shape that minimizes NCP aberrations without sacrificing potential science photons to maintain the NCP loop. In this scenario, maintaining a creep-free DM shape is desirable. By closing the loop on the NCP WFE for a time period before fixing the DM on the optimized shape, the effect of creep can be driven down. Fig. 12 shows the RMS creep for different choices of closed-loop time periods and for different levels of WFE. Each curve is the mean creep observed for five realizations of low-order (the first 10 Zernikes, neglecting piston) WFE. Longer closed-loop periods result in a more stable surface. At the expected 25 nm RMS NCP WFE for MagAO-X, a relatively short a 5-minute closed-loop period reduces shape creep to $\sim$ 1 nm RMS over an hour. Shape drift due to thermal variations in the dome will likely dominate over shape creep and may require periodically re-closing the loop on the NCP DM or else maintaining closed-loop operations at all times.

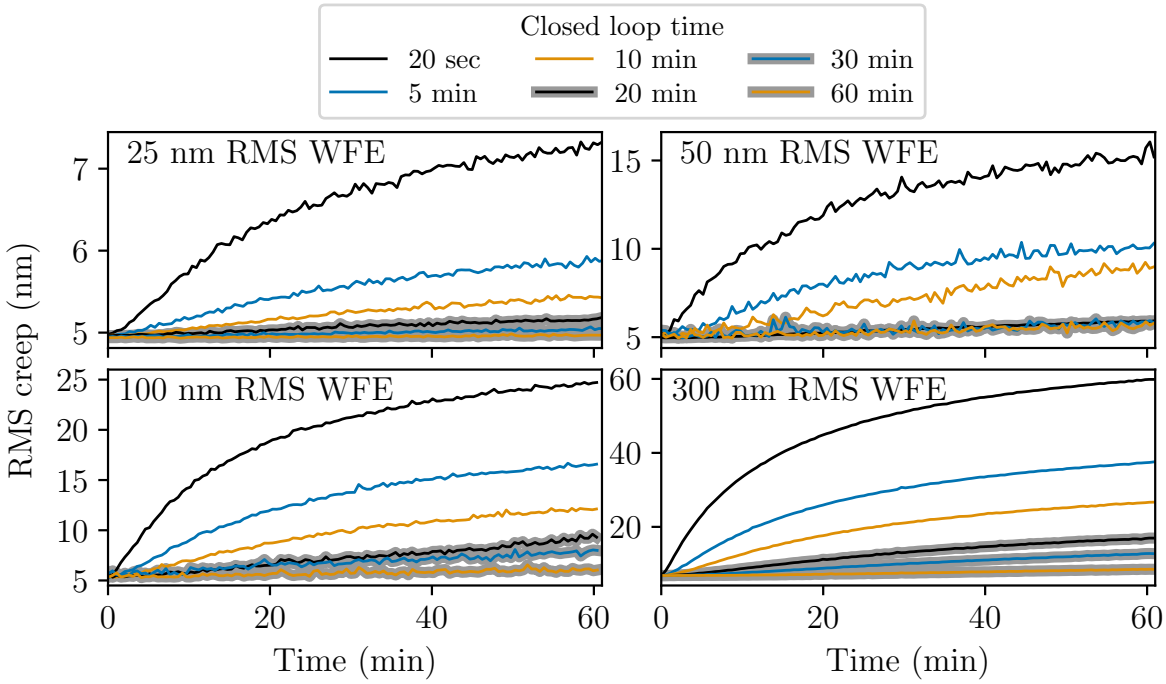

Fig. 12.—: ALPAO shape creep after opening the loop on (top left) 25 nm, (top right) 50 nm, (bottom left) 100 nm, and (bottom right) 300 nm RMS low-order wavefront errors on the DM. Each line shows the mean creep of 5 realizations of WFE after closing the loop on the shape for the indicated time period. Shape creep on the expected 25 nm RMS of NCP wavefront error can largely eliminated by closing the NCP loop for 5-10 minutes. The 5nm RMS floor arises from surface errors outside of the control bandwidth.

5. Instrument Strehl Optimization

To minimize static instrument aberrations that remain after alignment or arise due to optomechanical drift and to bring the wavefront sensors within their linear range, a simple algorithm was developed to maximize the instrument Strehl. To minimize aberrations seen by the pyramid wavefront sensor, an image of either the internal white light or laser source is formed on a Basler camera that picks off the beam right before the pyramid tip. The core of the PSF is measured as the woofer DM iterates over a precomputed modal basis set. As amplitude of each mode is varied in a grid search pattern, a quadratic polynomial is fit to the measured core to find the mode amplitude that maximizes the Strehl. An example curve for trefoil on the woofer DM is shown in Fig. 13. The search is performed mode-by-mode, and modes are revisited multiple times to reduce the effect of shape creep on the ALPAO. The same algorithm can be used to minimize NCP aberrations using the NCPC DM in conjunction with either the science cameras or the LOWFS camera.

This algorithm has proven successful in the lab. Optimized white light PSFs are shown in Fig. 14. The pyramid tip image is a broadband PSF over $\sim 0.65 - 1\mu$m. By comparison with a simulated broadband PSF formed by the Magellan pupil, the Strehl is estimated to be 67%. This calculation does not account for the focus chromatism of the white light source and is likely a pessimistic estimate of the instrument Strehl. The Strehl on the science camera is measured to be 86% in the Hα continuum filter.

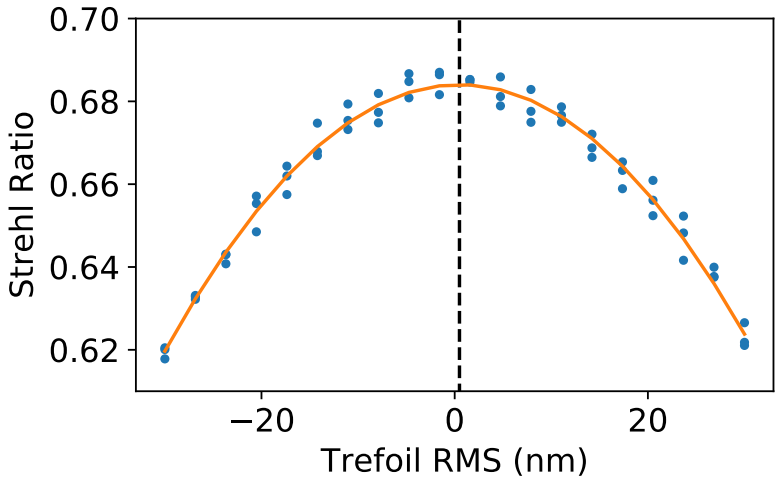

Fig. 13.—: Measured instrument Strehl as a trefoil mode is varied on the woofer DM. Measured data points are given in blue, while the best fit quadratic is plotted in orange. Repeating this procedure for 36 Zernike modes minimizes static instrument wavefront error.

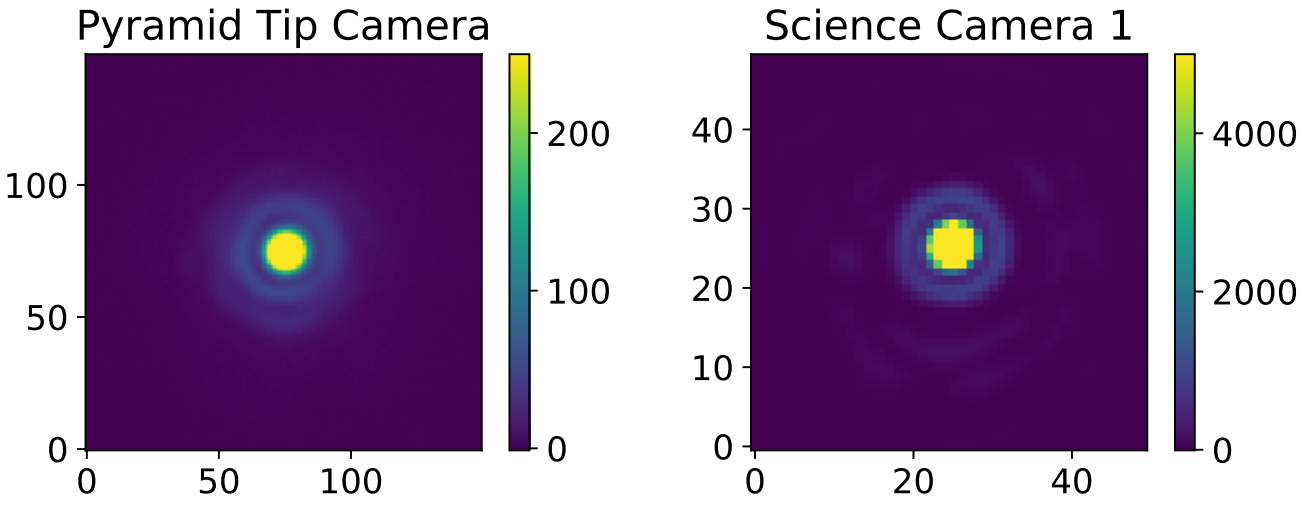

Fig. 14.—: Left: Measured white-light PSF at the pyramid tip over $\sim 0.65 - 1\mu$m. Right: Measured white-light PSF at the science camera in the Hα continuum filter. Strehls are reported in the text.